ORIGINAL PAPER



Apatite stability under different oxygen fugacities relevant to planetary bodies

Dustin Trail 1,2 1 · Yanling Wang 1

Received: 30 November 2017 / Accepted: 30 May 2018 © Springer-Verlag GmbH Austria, part of Springer Nature 2018

Abstract

Apatite is widely distributed in terrestrial and extraterrestrial environments and may therefore crystallize in relatively oxidized environments found here on Earth, and in reduced settings such as the Moon. We present a series of oxygen fugacity-buffered apatite stability and apatite-fluid solubility experiments conducted at 1 atm and in a piston cylinder, respectively. The first style of experiments involved enclosing polished slabs of Durango apatite in evacuated silica tubes with a solid-state oxygen fugacity buffer, followed by heating to ~1100 °C for 65 or 90 h. At oxygen fugacities equal to and lower than the Fe-FeO equilibrium, crystals revealed alteration often in the form of convoluted features, which may to be related to the stability of the apatite component P₂O₅ under reducing conditions. Preferential evaporation of P₂O₅ from a haplobasalt heated to 1350 °C under reducing conditions – compared to similar experiments conducted under oxidizing conditions – also supports this interpretation. Fifteen solubility experiments were conducted in a piston cylinder device at 900 or 925 °C and 1 GPa, in either ~3.4 N NaCl or 2 N NaOH fluids. The oxygen fugacity was buffered at about 4 log units below the favalite magnetite quartz equilibrium (FMQ-4) to 8 log units above this buffer (FMO + 8). Apatite solubilities were determined by crystal weight loss. There is no systematic sensitivity to solubility vs. oxygen fugacity in H₂O-NaOH fluid. In the H₂O-NaCl fluid, apatite is less soluble by about a factor of 2 under the most oxidizing experimental conditions. This change in solubility is relatively subtle when compared to intensive variables explored in other studies, such as temperature, pressure, and X_{NaCl} in the fluid. Overall, the apatite crystal structure is resilient across a range of different imposed oxygen fugacities, which contrasts with experimental results for another phosphate, monazite.

Keywords Apatite · Oxygen fugacity · Stability · Planetary · Solubility

Introduction

Apatite [Ca₁₀(PO₄)₆(OH, F, Cl)₂] is widely distributed on Earth and is a common accessory mineral found in igneous

Editorial handling: L. Nasdala

Electronic supplementary material The online version of this article (https://doi.org/10.1007/s00710-018-0602-y) contains supplementary material, which is available to authorized users.

☑ Dustin Trail dtrail@ur.rochester.edu

Published online: 14 June 2018

- Department of Earth & Environmental Sciences University of Rochester, 227 Hutchison Hall, Rochester, NY 14627, USA
- Department of Earth, Planetary and Space Sciences, University of California Los Angeles, 595 Charles Young Drive East, Los Angeles, CA 90095, USA

(mafic - felsic), metamorphic, and sedimentary rocks (Spear and Pyle 2002; Piccoli and Candela 2002; Belousova et al. 2002). It may also crystallize from high water activity fluids (e.g., Young et al. 1969) and is a common extraterrestrial mineral with known occurrences on the Moon, Mars, and 4 Vesta (Leshin 2000; McCubbin et al. 2011; Sarafian et al. 2013). Apatite may incorporate H-C-O-S species into its crystal structure, a characteristic used to explore past volatile abundances in terrestrial and planetary rocks (e.g., McCubbin et al. 2010; Marks et al. 2012; McCubbin et al. 2014). The large ionic radii of the VIICa and IXCa sites in apatite (Hughes and Rakovan 2002) indicate large ion lithophile elements – some of which are redox sensitive – may be compatible in the lattice. This is confirmed by detection of weight-percent levels of these cations (e.g., rare earth elements; REEs) in natural apatite and the large apatite/liquid partition coefficients determined in the laboratory (Watson and Green 1981; Belousova et al. 2002; Ayers and Watson

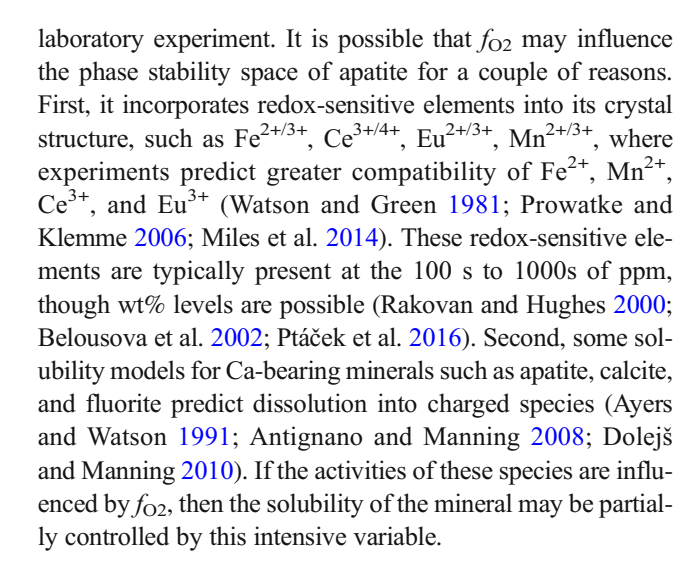


1993; McCubbin et al. 2011). Apatite also incorporates actinides, making it a frequent target of geochronology (Rakovan et al. 1997; Chew et al. 2014; Wohlgemuth-Ueberwasser et al. 2017) and thermochronology (e.g., Gleadow et al. 1986) investigations.

Its widespread occurrence, diverse chemistry, and potential applications to the study of planetary processes make apatite a frequent target of trace element and isotope studies, but it may also be a liability, unless knowledge of the stability and solubility under P-T-X conditions is well understood. Several earlier studies recognized this; for example, apatite solubility in silicate melts was shown to be primarily a function of temperature, SiO₂ content, and P₂O₅ content (Watson 1979; Watson 1980; Watson and Capobianco 1981). Subsequent work explored the alteration and solubility of apatite in aqueous fluids (e.g., Ayers and Watson 1991; Antignano and Manning 2008; Betkowski et al. 2016). Ayers and Watson (1991), for instance, showed that apatite solubility and mobility varied with fluid composition. Antignano and Manning (2008) demonstrated a positive correlation between solubility and pressure/temperature. They also noted a strong increase in solubility with rising NaCl mole fraction of the fluid, an observation that also holds for KCl-H₂O fluids (Mair et al. 2017). Betkowski et al. (2016) conducted experiments from 300 to 600 °C in alkali-rich fluids with monazite+apatite, and documented selective alteration of these minerals to other phases, such as vitusite and britholite. These studies help predict the occurrence and stability of apatite during fluid alteration, and they may also help facilitate the interpretation of apatite age and trace element information.

To the best of our knowledge, there is no work that has evaluated the stability and solubility of apatite as a function of oxygen fugacity (f_{O2}). Recent experiments have shown that another phosphate, monazite, undergoes incongruent dissolution in alkali-rich solutions at f_{O2} s equal to or greater than the fayalite-magnetite-quartz (FMQ) equilibrium (Trail 2018). Secondary phases with compositions along the CeO₂–ThO₂ join were found in some experimental products. In some respects, the investigation of apatite stability over a wide f_{Ω^2} range has broader applications than monazite, because apatite is found in reduced settings such as the Moon and 4 Vesta (McCubbin et al. 2010; Sarafian et al. 2013) and in more oxidized settings present on Earth. If these different planetary settings are considered, apatite may form or interact with geochemical reservoirs 2–4 log units below the iron wüstite (IW) buffer to the magnetite-hematite (MH) equilibrium (e.g., Sato et al. 1973; Pringle et al. 2013; Frietsch and Perdahl 1995). This covers an $f_{\rm O2}$ range of ~12 log units. Moreover, estimates of Mercury's mantle f_{O2} range from 2.3 to 6.3 log units below IW (Zolotov 2011; McCubbin et al. 2012), so even more reduced planetary settings are plausible.

The primary purpose of this contribution is to explore the stability and solubility of apatite as a function of f_{O2} by



Materials and methods

Samples

Durango apatite slabs were cut from a large crystal perpendicular to the c-axis. Slabs were attached to an aluminum disk with crystal bond and polished with 1 μ m alumina using a MiniMetTM automated polisher. After cleaning, they were finished with a final polishing step using a suspension of colloidal silica. Subsequently, slabs were scribed with a tungstencarbide tip, and then fractured to produce ca. 2 to 6 mg chips. The chips were inspected optically for inclusions or cracks. In a few cases, unpolished, unorientated Durango apatite fragments were used as starting material.

One atmosphere experiments

A series of simple one-atmosphere experiments was conducted to explore the stability of apatite at different oxygen pressures. This type of experiment was motivated by the $f_{\rm O2}$ -buffered olivine/pyroxene-basalt partitioning of several elements – including P – by Mallmann and O'Neill (2009). In this study, $f_{\rm O2}$ was buffered from FMQ-13.3 to FMQ+11.4 at 1 atm. Under conditions close to and below the iron-wüstite equilibrium, Mallmann and O'Neill (2009) documented systematic changes in the partitioning of P, and proposed the presence of P³⁺. If correct, the stability of apatite – or any phosphate mineral – may be affected at $f_{\rm O2}$ s close to or below IW. This hypothesis, was explored with two separate types of experiments.

In the first style of experiments, apatite stability vs. f_{O2} was explicitly assessed at 1 atm. The general experimental design is presented in other studies (e.g., Trail et al. 2013; Richter et al. 2014; Trail et al. 2016) which is briefly reviewed here (Fig. 1a). First, solid-state f_{O2} buffers (Si-SiO₂, Fe-FeO, Ni-



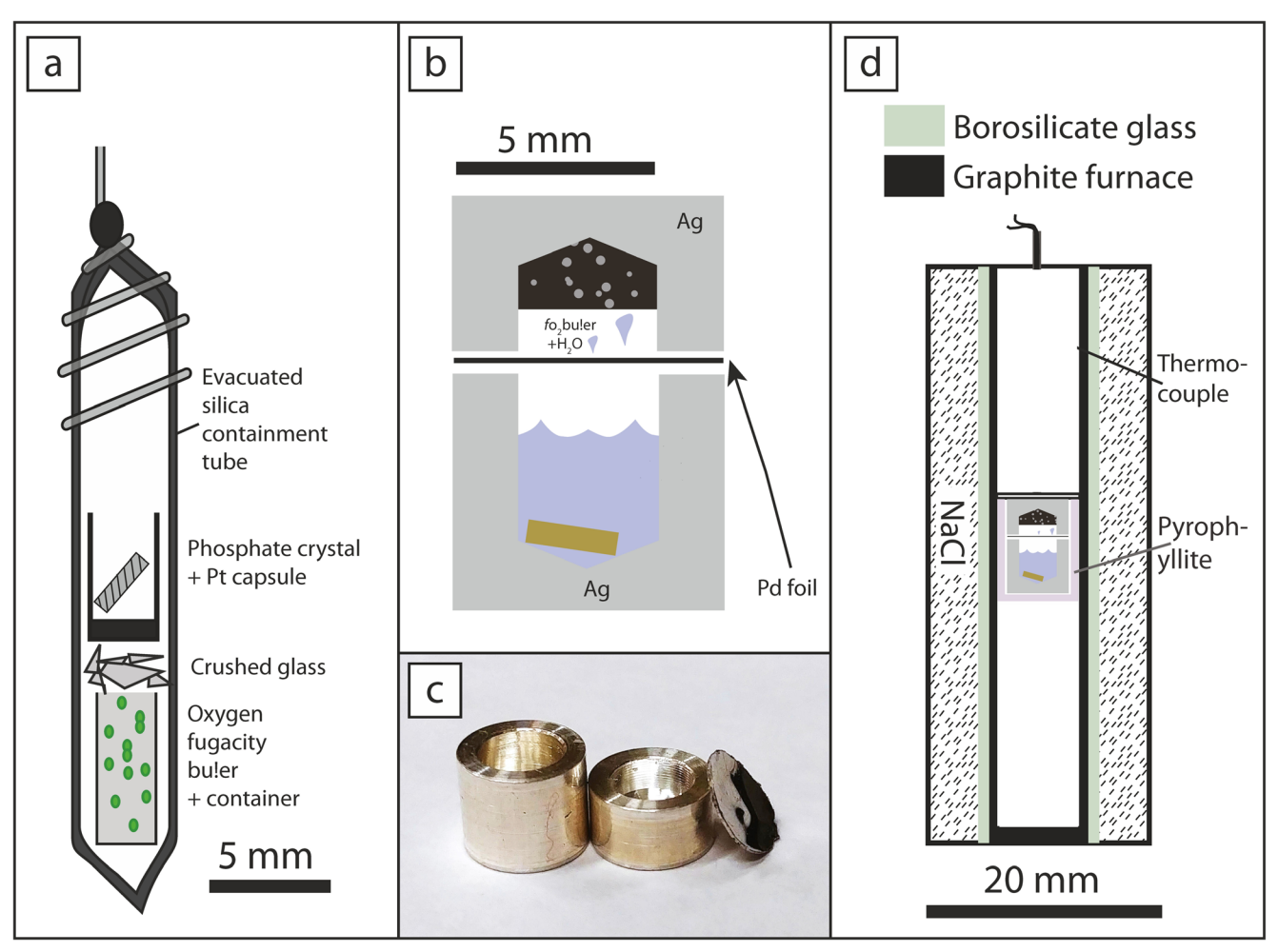


Fig. 1 a Schematic showing the experimental set-up of 1 atm, f_{O2} -buffered experiments. The f_{O2} buffers used were Si-SiO₂, C-CO-CO₂, Fe-FeO, Ni-NiO, Fe₃O₄-Fe₂O₃, ranging from ~FMQ-12 to FMQ + 5.8 at ~1100°C. The design is similar to that used in Richter et al. (2014) **(b)** Capsule configuration used for f_{O2} -buffered experiments conducted in a piston cylinder device, after the technique described in Trail (2018). The capsule rims contain concentric rings (tool marks) from machining. These are purposely left which help form a water-tight seal during pressure

sealing. $\bf c$ A photograph of the 2 capsules, with the Pd foil in the right of the image. The outer diameter of the Ag capsule is 7.4 mm. The $f_{\rm O2}$ is buffered by diffusion of H₂ through the Pd foil. The low profile, thickwalled capsule mitigates against thermal gradients and therefore vapor transport/recrystallization of dissolved solutes. $\bf d$ The NaCl-borosilicate cell design used in these experiments, with capsule positioned at the midpoint (length = 45 mm). The borosilicate glass acts as a thermal insulator

NiO, Fe₃O₄-Fe₂O₃) were ground dry, and then packed firmly into a 3 mm silica glass bucket. This was inserted into a 5 mm inner diameter silica glass tube with a sealed bottom. The CO-CO-CO₂ buffer was implemented by replacing the bucket with a 2 mm plug of graphite. Together, these f_{O2} buffers cover a range from about 12 log units below the fayalite magnetite quartz buffer (~FMQ-12) to 5.8 log units above this buffer (FMQ + 5.8), where the FMQ buffer is defined by Myers and Eugster (1983). Subsequently, shards of silica glass were placed on top of the buffer within the silica tube, followed by insertion of a Pt capsule containing a polished slab of apatite. Silica tubes were evacuated and sealed. The finished ampoules were placed in a 1 atm furnace pre-heated to ~1100 °C. Experiments were left to dwell for 65 or 90 h, and temperature monitored with a type-K thermocouple. The buffers are assumed to react with any residual O_2 in the ampoule,

thereby buffering the oxygen fugacity. The presence of $f_{\rm O2}$ -buffering phases was confirmed upon completion.

The second style of 1-atm experiments probed the volatility of apatite components vs. $f_{\rm O2}$ in a synthetic Fe-free haplobasalt. About 2 g of reagent-grade chemicals were well mixed by hand in a mortar and pestle in ethanol, and then dried underneath a heat lamp. The target composition can be found in Online Resource 1, which includes 29 wt% CaO, 6 wt% P_2O_5 , and 0.5 wt% F. About 50 mg of this mixture was packed into Pt capsules and placed in a silica tube. The tube was sealed with either a Ni-NiO or magnetite-hematite (MH) buffer using the same experimental design described in the previous paragraph (e.g., Fig. 1a). A separate experiment was prepared in a slightly different manner, which involved packing the rock mix directly into a machined graphite capsule, which was then inserted into the silica tube. All ampoules

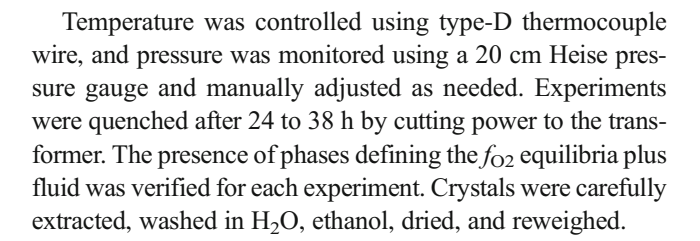


were placed into a 1 atm furnace pre-heated to 1350 °C, and T was monitored with a type-R thermocouple. At experimental conditions, the oxygen fugacities of the three experiments were FMQ-5.9 (graphite capsule), FMQ + 0.6 (Ni-NiO), and FMQ + 5.6 (MH). Note that these experiments were conducted above the liquidus to avoid conflating effects associated with the crystallization and partitioning of P, Ca, F into other minerals, including apatite. After 19 h, samples were drop-quenched simultaneously into a bucket of water. The $f_{\rm O2}$ -buffering phases were confirmed upon completion.

Hydrothermal solubility experiments

Apatite solubilities in fluids vs. f_{O2} were investigated using a modified version of the double capsule technique (e.g., Trail 2018). Six different f_{O2} buffers fixed the oxygen fugacity from ~4 log units below the fayalite-magnetite-quartz buffer (FMQ-4; Mo-MoO₂) to ~8 log units above the FMQ equilibrium (FMQ + 7.9; Ru-RuO₂). Our design uses two thick-walled Ag capsules, machined from a solid 7.35 mm 99.9% pure Ag rod, with an apatite chip and experimental fluid placed in one, and the buffer (+H₂O) placed in the other. This design been shown to yield comparable solubilities, independent of experiment duration. For example, FMQ-buffered monazite solubility experiments conducted in 2 N NaOH fluid at 925 °C for 24, 70, and 188 h yield respective solubilities of 0.19 ± 0.03 , 0.18 ± 0.028 , and 0.20 ± 0.025 wt% (Trail 2018). During the experiment, the capsules are separated by an H₂-permeable Pd membrane (Fig. 1b,c). The thick-walled capsules limit the thermal gradient and mitigate against C infiltration into the capsule from the graphite furnace (Watson 1987; Brooker 1998).

Apatite chips were dried, weighed, and placed into the capsule with 60 µL of pre-mixed 2 N NaOH or ~3.4 N NaCl solution added with a microsyringe. This corresponds to a mole fraction of $X_{NaOH} = 0.035$ and $X_{NaCl} = 0.058$. The buffer capsule was packed firmly with about 40 mg of pre-mixed buffer material, followed by the addition of ~5 mg of water. The circular Pd foil was placed on top of the apatite-hosted capsule. The buffer capsule was then inverted and placed on top of the Pd foil. The experimental cell (Fig. 1d.) was cold sealed by pressurizing the samples to 1 GPa, followed by heating to 900 or 925 °C at a rate of 100°/min. These temperatures were selected in part because they are within the experimentally calibrated range of f_{O2} buffer equilibria. The temperatures were also sufficiently below the melting point of Ag at 1 GPa (960 °C 1 atm; 1020 at 10 kbar; Mirwald and Kennedy 1979), though high enough to facilitate solubility measurements by the crystal weigh loss method using a Sartorious CPA225D balance. The estimated precision is ~0.01 mg (1 s) based on repeated re-weighings over the course of this study and Trail (2018). This precision about an order of magnitude smaller than the apatite weight loss expected from past studies for the fluid volume, T, and P (Antignano and Manning 2008).



Analytical techniques

Durango apatite slabs were pre-characterized for REE concentrations with a Photon Machines 193 nm G2 laser ablation (LA) system equipped with a HelEx 2-volume sample chamber connected to an Agilent 7900 inductively coupled plasma mass spectrometer (ICP-MS) quadrupole. A laser fluence of 5 J/cm² with pulse rate of 10 Hz was used for 20 s of total ablation time using a 35 μ m spot. The data were reduced using Iolite 3.1® (Paton et al. 2011). Phosphorus was used as an internal standard, and concentrations were calculated by standardizing against NIST610 glass (Online Resource 2).

Doped haplobasalt glasses formed by fusion at 1350 °C were characterized with a Cameca SX 100 electron probe microanalyser (EPMA) with previously described procedures (Trail et al. 2012; Boehnke et al. 2013). Briefly, data were collected using an accelerating voltage of 15 kV and a defocused beam of 30 µm. All elements except P, F, and S were standardized against fused AGV-1 obtained from the United States Geological Survey. Fluorine and P were standardized against natural fluoro-topaz (F), and synthetic CePO₄, respectively. Sulfur was standardized against BaSO₄ (NNO- and MH-buffered experiments) or FeS₂ (CCO experiment). Sodium, Mg, Al, and Si K_{α} X-rays were collected through TAP crystals while S, K, P, Ca, and Ti K_{α} X-rays were collected through large PET crystals. Iron K_{α} X-rays were measured through a large LIF crystal. A beam current of 7 nA was used for all elements except S (15 nA) and elemental concentrations were calculated after counting for 10 s on peak and 4 s on backgrounds.

Surface morphologies of apatite crystals were documented using a Zeiss Auriga scanning electron microscope (SEM). Afterwards, crystals were mounted in epoxy – with the c-axis perpendicular to the surface – and polished to 0.3 µm with an Al₂O₃ slurry in preparation for follow-up electron beam investigations. Cross-sectioned slabs were imaged by SEM, and then polished again to expose a fresh surface in preparation for chemical analysis by EPMA. A carbon coat of ~200 Å was applied to the surface of the samples which matches the carbon coat thickness of the standards. The chemistry of the apatite rims and cores were quantified with JEOL JXA-8200 EPMA broadly following the procedures developed by Stormer et al. (1993) and Goldoff et al. (2012). All samples were analyzed with the c-axis perpendicular to the electron beam, an accelerating voltage of 10 kV, 6 nA beam current, and a 10 µm defocused spot. Fluorine, Cl, Ca, and P were



analyzed for 10 s on peak and 4 s on backgrounds using LDE1, PETH, PETH, and PETJ crystals, respectively. The elements were standardized against natural fluoro-topaz (F), synthetic $Ba_5(PO_4)_3Cl$ (Cl), and Durango apatite (P,Ca). Each crystal was analyzed at least 6 times.

Results

One atmosphere experiments

The SEM images reveal various surface features that developed during the experiment (Fig. 2). As a point of reference, Fig. 2a presents a secondary electron (SE) image of a typical slab, pretreatment, which is free of observable surface imperfections. The most reduced experimental product (\sim FMQ-12; Si-SiO₂) contains a mottled crystal surface accompanied by neo-formed CaSiO₃ when viewed in cross section (Fig. 2b). Possible model reactions are Ca₁₀(PO₄)₆(F)₂ \rightarrow CaF₂ + 9CaO + 3P₂O₅, followed by CaO + SiO₂ \rightarrow CaSiO₃, though no P/F phases were observed. This implies loss (volatilization) of P and F to the inside of the silica ampoule under these extremely reducing conditions. Apatites buffered at C-CO-CO₂ (FMQ-5.3) and Fe-FeO (FMQ – 3.7) exhibit convoluted textures on the grain surfaces, though

Fig. 2 Scanning Electron Microscope (SEM) images showing surface features; samples are viewed with the electron beam parallel to the c-axis of the crystal. a Example secondary electron (SE) image of an untreated polished slab, b The most reduced experimental product, sectioned and shown in cross section with the e-beam perpendicular to the c-axis. The backscattered electron image reveals that the surface is altered extensively, and contains neo-formed CaSiO₃. (c-d) Mottled surface textures persist at f_{O2} s of FMQ-5.3 and FMQ-3.7. respectively. The brighter regions in both secondary electron images are related to surface roughness and/or slight surface charging; no secondary phases were identified. e Minor recrystallization on the slab surface is evident for the experiment buffered at Ni-NiO. f. No detectable difference - when compared to the starting slab was noted for the sample buffered at the magnetite-hematite equilibrium

no secondary phases were detected (Fig. 2c,d). At Ni-NiO, the apatite surface exhibits only weak recrystallization, and no evidence for alteration of any kind is present at the MH equilibrium (Fig. 2 e,f). Thus, the main observation is that apatite is less stable under more reducing conditions, which is most pronounced at oxygen fugacities at or below the iron-wüstite equilibrium (Table 1).

Electron probe micro-analyser data of the three haplobasalt glasses buffered at different oxygen fugacities are summarized in Online Resource 1. This reveals that the P content in the glass – but not F or Ca – is significantly depleted in the sample that was buffered at FMO-5.9 (Fig. 3).

Apatite solubility in aqueous fluids vs. f_{02}

When compared to the initial surfaces (e.g., Fig. 2a), experimental products show evidence for dissolution at the crystal surfaces (Fig. 4). In some cases, mottled features are present on the crystal surfaces (Fig. 4a), while in others wavy or convoluted features exist (Fig. 4b-d). When crystals were aligned, mounted, sectioned, and polished perpendicular to the *c*-axis, evidence for dissolution/re-precipitation and new growth to 10s of µm deep is evident, which sometimes coincides with convoluted features near the rims of crystals (Fig. 4h-j).

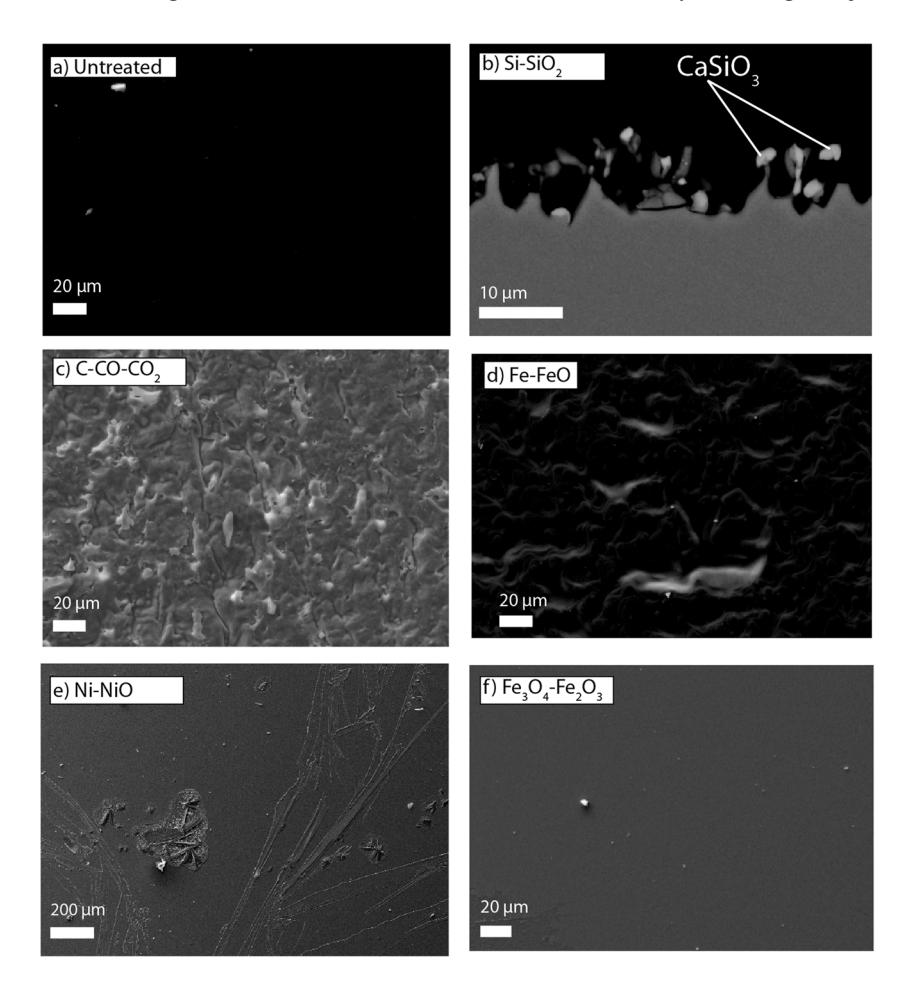




Table 1 Apatite 1 atm fo2-buffered heating experiment conditions observations on apatite grain surfaces

Experiment ID	T (°C)	t(h) ^a	fo ₂ buffer	ΔFMQ^b	Post experiment observations on apatite grains
PhB01_Ap_CCC	1083	90	C-CO-CO ₂	-5.3	Mottled surface features, possible loss of P
PhB01_Ap_HM	1083	90	Fe_3O_4 - Fe_2O_3	+5.8	No identifiable change to crystal surface
PhB01_Ap_IW	1083	90	Fe-FeO	-3.7	Topographic highs/lows surface alteration
PhB01_Ap_NNO	1083	90	Ni-NiO	+0.7	Regions of apatite recrystallization visible on surface
$PhB04_Ap_SiSiO_2$	1083	65	Si-SiO ₂	~-12	CaSiO ₃ + apatite and probable loss of P

^a Duration of the experiment in hours

Changes in backscattered electron image (BSE) brightness reveal defined boundaries between the original crystal and the altered region in some images (e.g., Fig. 4j). Also present are infrequent $\sim 1-5~\mu m$ blebs of Ag mobilized during the experiment. While these Ag blebs will lead to undetectable mass additions to the crystal during post experiment reweighing, (Online Resource 3), they mark the termination of the dissolution-reprecipitation front of the crystal. In some cases, this is obvious (Fig. 4f,h); the Ag blebs correlate with the precise location of BSE brightness change. This provides strong evidence that partial or full recrystallization of the outer portion of the crystal occurred in at least some cases.

Almost all experiments were conducted with polished slabs and at 925 °C. We report two additional experiments at 900 °C, 1 GPa, with the $f_{\rm O2}$ buffered at FMQ, with unpolished, unorientated Durango apatite fragments. In the NaOH-H₂O solution, secondary ThO₂ was discovered on the surface of the

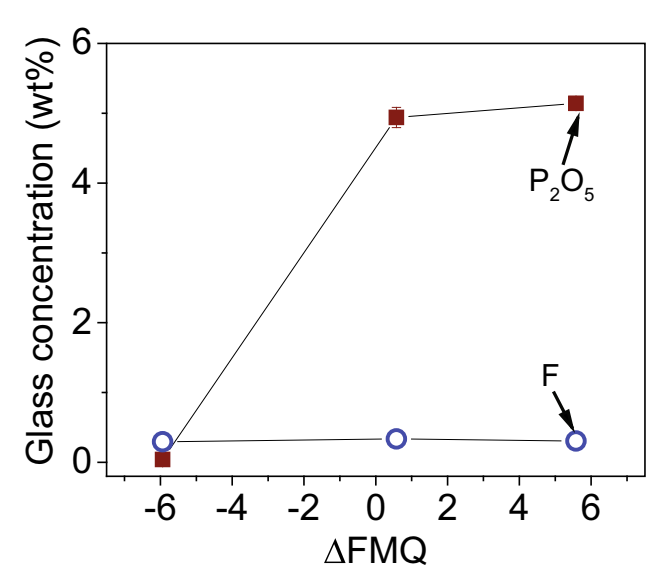


Fig. 3 Concentrations of F and P_2O_5 post-experiment in silicate glass (1 atm, 1350°C) showing that P_2O_5 is lost under reducing conditions. This supports the hypothesis that P-oxide is more volatile under very reducing conditions, and is also consistent with surface features documented for 1 atm apatite stability experiments. Fluorine and CaO do not show diminished concentrations vs. f_{O2} (also see Online Resource 1)

sample (Fig. 3f) whereas the NaCl-H₂O experiment contained secondary monazite.

Table 2 presents the apatite solubility results for the two different fluids. In NaOH fluid, apatite solubility exhibits no systematic change as $f_{\rm O2}$ was varied from FMQ-4 to FMQ + 7.9 (Fig. 5a). For these 8 experiments, the average solubility is 0.12 ± 0.02 (1 s.d.) wt%. This contrasts with solubility experiments conducted in the NaCl solution (Fig. 5b). Apatite solubility is largest between $f_{\rm O2}$ s from FMQ-4 to FMQ, with an average solubility of 0.20 ± 0.01 (1 s.d.) wt%. Interestingly, the measured solubility decreases to 0.16 ± 0.02 wt% at FMQ + 2.8 and then down to 0.09 ± 0.02 wt% at FMQ + 7.9.

Table 2 also presents the ratio of EPMA F and Cl rim concentrations, compared to the crystal core. Note that all concentrations reported were collected with the electron beam perpendicular to the c-axis of the crystal. A complete summary of all the EPMA concentrations can be found in Online Resource 4, which shows that the interior regions of the crystals remain undisturbed at the limits of analytical precision. In other words, the concentrations of Ca, Na, P, Cl, and F in the interior regions are in strong agreement with published literature values for Durango apatite (Young et al. 1969; Stormer et al. 1993; Goldoff et al. 2012).

More than half the F was lost from crystal rims in almost all cases. Apatite F depletion in experiments conducted in NaOH fluids exceeds that of the NaCl solutions, on average. Experiments conducted in NaCl solutions contain apatite Cl normalized concentrations comparable to core regions of the crystals, whereas the experimental products of NaOH fluid experiments are Cl-depleted. No systematic dependence for Cl/F exchange vs. oxygen fugacity is evident; charge balance arguments do require gain of OH in the reacted rims of the crystals, however.

Discussion

One atmosphere experiments

The main goal of the 1 atm experiments was to evaluate apatite thermal stability in simple f_{O2} -buffered environments. F-



^b Difference in log units from the fayalite-magnetite-quartz equilibrium buffer

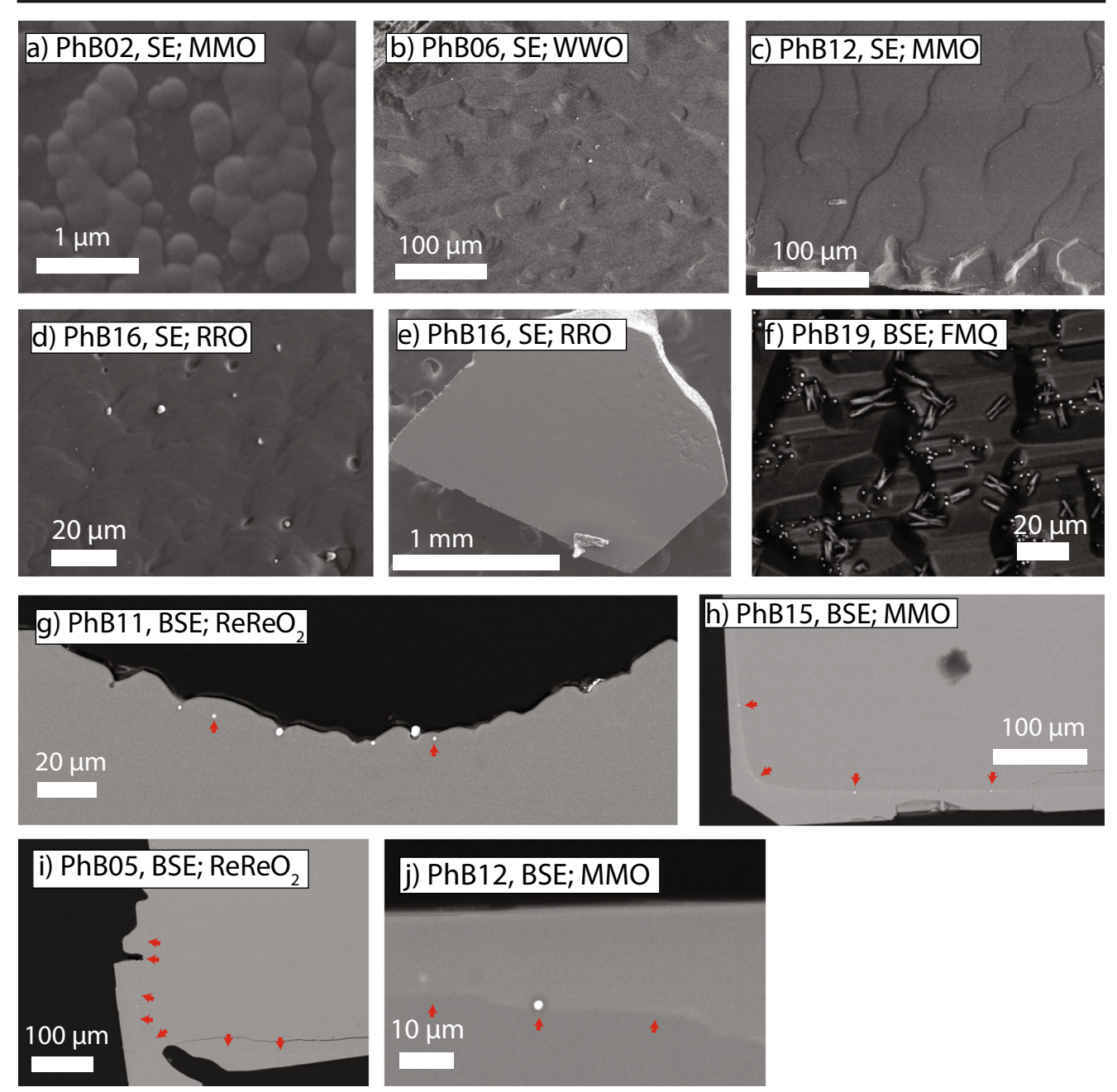


Fig. 4 SEM images showing textures of the apatite slabs after completion of piston cylinder experiments. Crystal slabs were prepared in the same manner as the 1 atm experiments, so the secondary electron (SE) image shown Fig. 2a is representative of the initial state of the apatite crystals. ad Representative textures of the crystal surfaces, with the electron beam parallel to the c-axis. SE images also show traces of Ag on the crystal surface (e.g. d). e Representative overview image of crystal slab, after completion of the experiment (electron beam parallel to the c-axis). f Backscattered election image of unorientated, unpolished apatite

fragment. The phases with high aspect ratios are apatite, interpreted to form on the quench. The BSE bright phases are ThO2. **g-j** Slabs were mounted and polished to expose the crystal surfaces in cross section, which reveal alteration of the original mineral to tens of μm deep. Small blebs of Ag, identified by the arrows, are found within the apatite, and near the apparent termination of the reaction boundary. In this case, all crystals are viewed with BSE and the electron beam perpendicular to the c-axis of apatite

apatite was predicted to be stable in air at the ~ 1100 °C temperature investigated conducted here (Tõnsuaadu et al. 2011). This previously documented stability agrees with the most oxidized experiments presented here, in which the oxygen pressure was fixed at the MH equilibrium, or $\sim 10^{-4}$ bars.

However, the qualitative observations of crystal surfaces demonstrate breakdown and alteration of apatite for oxygen fugacities at or more reduced than the IW equilibrium. We speculate that the reduction of P^{5+} to P^{3+} is responsible for this instability. This is consistent with the 1 atm f_{O2} -buffered experiments



Apaite-fluid solubility experiment conditions and results on apaitte compositions and mass changes during runs Table 2

Molality (mol/kg) ^f	0.0024	0.0018	0.0028	0.0028	0.0028	0.0024	0.0021	0.0021	0.0015	0.0040	0.0032	0.0040	0.0017	0.0037	0.0035
Phases present	I	I	I	I	I	I	ı	ı	Th-oxide	ı	ı	I	I	I	Monazite
Apatite preparation	Polished ⊥	Polished 1	e Polished⊥	Polished 1	e Polished ⊥	Polished ⊥	e Fragment	Polished \perp	c Fragment	Polished \bot	${\bf c} \\ {\bf Polished} \perp$	c Polished⊥	e Polished⊥	e Polished⊥	c Fragment
1 s.d. ^e	0.02	0.02	0.02	0.02	0.02	0.02	0.02	0.02	0.02	0.02	0.02	0.02	0.02	0.02	0.02
Apatite solubility (wt%) ^d	0.12	60.0	0.14	0.14	0.14	0.12	0.11	0.11	0.08	0.20	0.16	0.20	60.0	0.19	0.17
Final apatite wt (mg)	4.66	2.25	4.23	2.16	2.23	1.84	2.72	3.55	2.94	5.56	4.48	4.55	5.83	3.71	5.57
Fluid added (µL)	09	09	09	09	09	09	09	09	09	09	09	09	09	09	09
Initial apatitewt (mg)	4.74	2.31	4.32	2.25	2.32	1.92	2.79	3.62	2.99	5.70	4.59	4.69	5.89	3.84	5.69
Starting fluid comp.	2 N NaOH	2 N NaOH	2 N NaOH	2 N NaOH	2 N NaOH	2 N NaOH	2 N NaOH	2 N NaOH	2 N NaOH	3.4 N NaCl	3.4 N NaCl	3.4 N NaCl	3.4 N NaCl	3.4 N NaCl	3.4 N NaCl
ΔFMQ^c	-4.00	2.78	-2.70	-2.12	7.97	0.00	7.97	2.78	0.00	-4.00	2.78	-4.00	7.97	0.00	0.00
\int 62	Mo-MoO ₂	$Re-ReO_2$	$W-WO_2$	FeO-Fe ₃ O ₄	Ru-RuO ₂	FMQ	Ru-RuO ₂	$Re-ReO_2$	FMQ	Mo-MoO ₂	Re-ReO ₂	Mo-MoO ₂	Ru-RuO ₂	FMQ	FMQ
t(h) ^b	38	38	38	38	38	38	38	27	24	27	24	27	27	24	24
1 s.d.	0.12	90.0	0.20	0.08	90.0	0.28		90.0		0.10	0.19	0.11	0.14	0.37	
Cl_rim/ Cl_core ^a	0.99	0.07	0.30	0.15	0.35	0.70	n.m.	0.23	n.m.	0.78	1.14	1.04	09.0	1.15	n.m.
1 s.d.	0.04	0.01	90.0	0.05	0.07	0.04		0.05		0.04	80.0	0.11	0.05	80.0	
F_rim/ F_core ^a	1.04	0.05	0.37	0.25	0.35	0.61	n.m.	0.40	n.m.	0.50	0.70	29.0	0.54	9.00	n.m.
T (°C)	925	925	925	925	925	925	925	925	006	925	925	925	925	925	006
Exp	PhB02	PhB05	PhB06	PhB07	PhB08	PhB09	Phb10	Phb11r	PhB19	Phb12	Phb13	Phb15	Phb16	Phb18	PhB20

^a Concentration ratio of the rim to core region of the apatite, measured at the completion of the experiment

^b Duration of the experiment in hours

^c Difference in log units from the fayalite-magnetite-quartz equilibrium buffer

^d Solubility represented as wt% apatite dissolved in the fluid ([wt loss of crystal/wt of fluid] × 100), using a density of 1.08 g/ml for 2 N NaOH or 1.1478 g/ml for 3.4 N NaCl

^e Propagated uncertainty based on 3–7 measurements of initial and final crystal weight

^fMolality of apatite dissolved in fluid; calculated with F-apatite and moles of solute per kg of mixed solvent



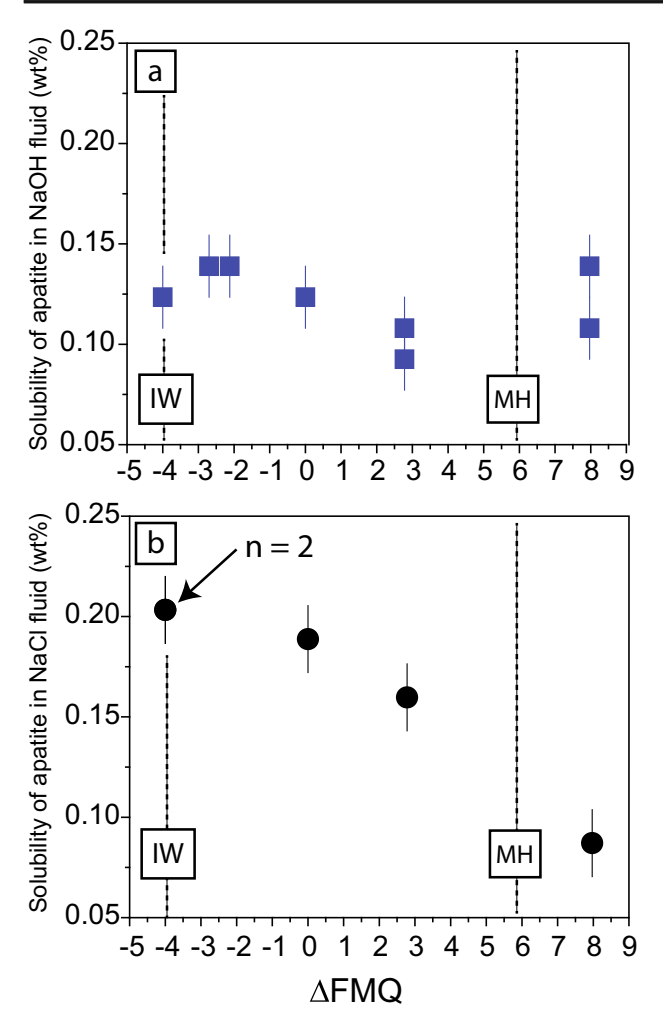


Fig. 5 a Solubility of apatite in NaOH solution, represented as wt% apatite dissolved in the fluid, showing no resolvable sensitivity to oxygen fugacity. The x-axis represents the difference in log units relative to the FMQ oxygen fugacity buffer. **b** Solubility of apatite in NaCl solution showing that apatite is more soluble by about a factor of two in highly oxidizing experiments

conducted by Mallmann and O'Neill (2009). These workers argued for the presence of P^{3+} at f_{O2} s of FMQ-5 and lower, based on apparent changes in P partition coefficients between mantle phases and basaltic melt. We also speculate that P^{3+} is more volatile than P^{5+} since simple f_{O2} -buffered basalt experiments conducted here show almost complete loss of P from the melt under reducing conditions (FMQ-5.9).

It is important to iterate that these experiments were not designed to specifically evaluate equilibrium conditions, or to define an equilibrium reaction. They were designed to assess the stability of apatite and its components with changes in oxygen pressure. In this regard, anhydrous results imply apatite stability is unlikely to be affected by $f_{\rm O2}$ s common in any present-day terrestrial settings. In planetary settings where the $f_{\rm O2}$ is close to the IW equilibrium or below, these data indicate apatite is less stable. From a planetary perspective, basaltic

eruptives that were exceptionally reduced may have delayed or inhibited apatite saturation. Such conditions may be possible on Mercury or the Vesta 4 based on recent $f_{\rm O2}$ estimates of these bodies (Pringle et al. 2013; Zolotov 2011), though they are less likely on the Moon or Mars.

Apatite-fluid solubility experiments vs. oxygen fugacity

Comparison with other apatite solubility results

Figure 6 presents apatite solubility data conducted in NaCl- $\rm H_2O$ at 1 GPa, and variable temperature. This consists of 2 data points representing the effects of apatite solubility in fluids vs. $f_{\rm O2}$ from Table 2, and several of the solubility results from Antignano and Manning (2008), who parameterized T, P, and $\rm X_{\rm NaCl}$ of their apatite solubility data. Those experiments were not explicitly $f_{\rm O2}$ -buffered, though they were likely close to the Ni-NiO equilibrium (Newton and Manning 2005; Tropper et al. 2011). Our experiments conducted at oxygen fugacities from FMQ-4 to FMQ are in broad agreement with the previous results of Antignano and Manning (2008). On the other hand, the measured RRO-buffered apatite solubility is lower than those reported for more reduced experiments. To explore the implications of this result, we use the following

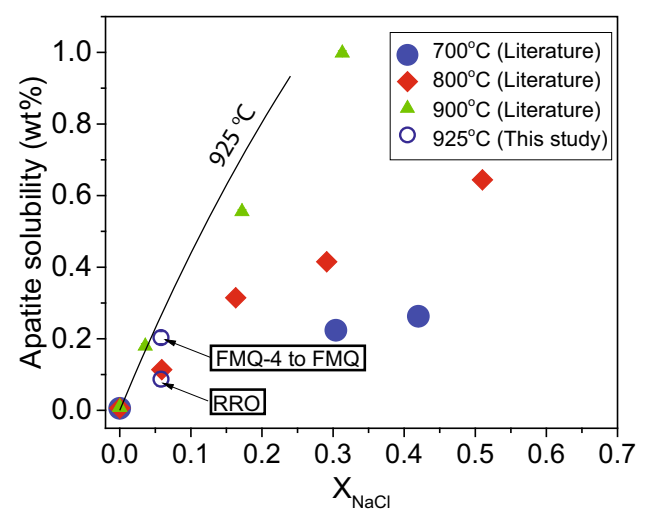


Fig. 6 Apatite solubility (1 GPa) experiments from Antignano and Manning (2008) (Literature) and this study showing how $f_{\rm O2}$ changes solubility, in comparision to experiments conducted at different temperatures, where $X_{\rm NaCl}$ is mole fraction. The oxygen fugacity of experiments conducted by Antignano and Manning (2008) were probably close to the NNO equilibrium. A change in the oxygen fugacity from FMQ to FMQ + 2.8 would have the same effect as a 30° temperature change at ~900°C, whereas a change in oxygen fugacity from FMQ to the most oxidized experiment conducted (Ru-RuO₂) is equivelent to about a ~120° change in temperature. Note that this generalized comparison only applies at 900°C and $X_{\rm NaCl}$ = 0.0582; that is, there is not enough data to speculate on how this might change as other intensive variables are investigated



parameterized fit that describes a patite solubility (C_{ap} , in ppm) in NaCl fluids:

$$c_{ap} = -3.56 + .002421T + 9.17\log(\rho_{H_2O}) + [(4.4 + 1.1P^4)exp(0.007T)] \times (a_{NaCl})^{1/2}$$
 (1)

where T is in Kelvins, ρ_{H2O} is the density of water, P is pressure in GPa, and a_{NaCl} is the activity of NaCl in solution (Antignano and Manning 2008). The a_{NaCl} of the solution is defined by:

$$a_{NaCl} = \frac{4(X_{NaCl})^2}{(1 + X_{NaCl})^2}$$
 (2)

where X_{NaCl} is the mole fraction of NaCl in solution (Aranovich and Newton 1996). When this fit is performed on our data, treating T as an unknown, the FMQ-4 to FMQ data predict an experiment temperature of ~885 °C, which is lower than the true experimental temperature by 40 °C, but in broad agreement with previous results. Instead, if the same calculation is conducted for the oxidized experiment, the predicted experimental temperature is ~765 °C. In other words, the difference in apatite solubility that results from changing the experiment oxygen fugacity from FMQ to RRO is equivalent to the same change in solubility that would result from a 120 °C change in temperature (holding P and X_{NaCl} constant).

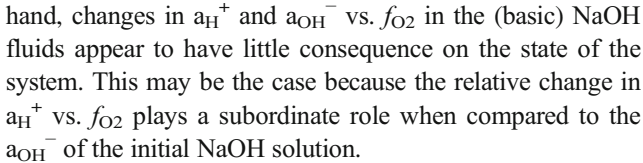
The reason for the decrease in solubility in NaCl fluids at high f_{O2} s is not clear, though it is reasonable to assume that the activities of the solute complexes that form during dissolution may depend on oxygen fugacity. For instance, the reaction $H_2 + \frac{1}{2}O_2 \leftrightarrow H_2O$ is important for buffering the oxygen fugacity, and furthermore, $high\ f_{O2}$ implies $low\ f_{H2}$. Consider for a moment the half-cell reaction $\frac{1}{2}H_2 \leftrightarrow H^+ + e^-$, which implies that the activity of H^+ (H^+) in the fluid may be lower at high H^+ (H^-). Starting then with the simple model reaction:

$$Ca_5(PO4)_3 F(solid) = 5 Ca^{2+} + 3 PO_4^{3-} + F^-$$
 (3)

and assuming the phosphate ion interacts with H^+ in solution implies the following series:

$$PO_4^{3-} + H^+ \rightarrow HPO_4^{2-} + H^+ \rightarrow H_2PO_4^{-} + H^+ \rightarrow H_3PO_4$$
 (4)

where the reactions are driven to the right with high a_H^+ (low f_{O2}) thereby leading to higher apatite solubilites. The reaction is driven to the left with low a_H^+ (high f_{O2}), implying lower apatite solubilities. Thus, if a_H^+ is involved in reactions that define the dissolution complexes for apatite and the model reactions are valid, this explains the diminished solubility detected at higher f_{O2} s. Dissolution and ion complexing that involve H^+ are supported by Ayers and Watson (1991), who showed that apatite weight loss was higher in HCl solutions (vs. NaCl) for identical experimental conditions. On the other



Antignano and Manning (2008) observed secondary monazite during their Durango apatite dissolution experiments in all experimental products ($\rm H_2O$ and $\rm H_2O$ -NaCl fluids). Despite intensive searches for monazite resulting from incongruent dissolution in our 925 °C experiments, none were observed. The reason for this is unknown, but could be due to differences in apatite chemistry among the Durango apatite suite, or the slightly higher temperatures explored here (925 °C) vs. maximum 900 °C temperatures of the former study. Ayers and Watson (1991) did not comment on monazite formation in their higher temperature, 1000 °C, 1 GPa Durango apatite solubility study in NaCl either.

The apparent absence of monazite in our run products may also be because the flat polished surfaces or our crystal slabs were poor retainers of secondary phases compared to rougher surfaces. Two separate experiments were conducted with unpolished, unorientated grains at 900 $^{\circ}$ C and 1 GPa, which yield secondary monazite and ThO₂ in NaCl- and NaOH-bearing fluids, respectively. The former is consistent with past observations, though no comparison is possible for NaOH fluids because no previous studies have explored apatite solubilities in NaOH-H₂O.

Implications of apatite-fluid experiments

These experiments enable an evaluation of apatite solubility with consideration for another variable, oxygen fugacity. While apatite in the presence of NaOH fluids shows little sensitivity to changes in solubility, previous work demonstrated that monazite is less stable in the presence of oxidized fluids with the same composition (Trail 2018). Therefore, in oxidized hydrothermal environments where NaOH may be an important component, such as in granitic pegmatites (Hetherington and Harlov 2008; Hetherington et al. 2010; Harlov et al. 2011) or high-grade mineral alteration of apatite in alkali-rich fluids (Bingen and van Breemen 1998; Förster and Harlov 1999; Hetherington and Harlov 2008), apatite will likely be more stable than monazite. As researchers continue to test hydrothermal mineral replacement reactions, such as those conducted for apatitemonazite pairs (Harlov et al. 2005; Betkowski et al. 2016), it is reasonable to expect that the products of these reactions are also likely to depend on f_{O2} .

On the other hand, the solubility of apatite in NaCl fluid does change with $f_{\rm O2}$. While salinity is interpreted to be an important agent involved in rock alteration and mass transfer (Newton and Manning 2010; Manning and Aranovich 2014), our results suggest that more oxidized



NaCl-H₂O fluids would diminish rare earth element mass transfer involving apatite, if the lower solubilities reported here are used. In natural settings, textures and analyses of apatite show that REEs and halogens are not preserved near the rims during interactions with briny fluids (e.g., Zhang et al. 2017). The occurrence of apatite in diverse environments extends the applicability of these results beyond terrestrial settings. Consider, for example, the results of Sarafian et al. (2013) who quantified the chemistry of eucritic apatite, some of which contain abundant OH found in the presence of quartz. Together, those results were used to suggest interactions of hydrothermal fluids with the early crust occurred on 4 Vesta. Finally, Rigali et al. (2016) made the case for using apatite as a radioactive waste repository phase, provided additional experiments are as encouraging as those published thus far. The results presented here strengthen this prospect, given that oxidized fluids stabilize apatite. That said, the apatite structure mineral Belovite-(Ce) (Rakovan and Hughes 2000) is likely to have a different response to oxidized fluids than Durango apatite.

Conclusions and outlook

When compared to observations made for monazite, apatite exhibits remarkable stability in extremely oxidized or reduced fluids, though on balance it is more stable in oxidized settings. In this regard, apatite may be a better phosphate to target for the development of f_{O2} sensors for fluids and melts, especially in oxidized environments. Under the most reduced conditions, apatite stability is adversely affected, as shown for the 1 atm experiments. Phosphorus exhibits volatile behavior under very reducing conditions. These experiments show the mobility of REE and P from the dissolution of apatite will be inhibited under oxidizing conditions in the presence of NaCl fluids, though compiled data indicate that P, T, and fluid composition are more important intensive variables. Since apatite does exhibit some sensitivity to changes in solubility vs. f_{O2} , a reasonable inference is that the speciation of dissolved components (or their activities) may depend on f_{O2} . There is value in exploring solubilities of other phases as a function of f_{O2} , even for minerals that do not contain redox-sensitive elements as part of their formulae.

Acknowledgements We thank Jacob Buettner for assistance. Rosario Esposito is thanked for assistance with the EPMA at UCLA. Haplobasalt glasses were characterized by EPMA at Rensselaer Polytechnic Institute. This work was supported by EAR-1447404 and EAR-1751903. The LA-ICP-MS instrument is partially supported by a grant from the Instrumentation and Facilities Program, Division of Earth Sciences, NSF (EAR-1545637). Dan Harlov, Peter Tropper, James Webster and an anonymous reviewer are thanked for comments and suggestions that greatly improved the manuscript.

References

- Antignano A, Manning CE (2008) Fluorapatite solubility in H_2O and H_2O -NaCl at 700 to 900 °C and 0.7 to 2.0 GPa. Chem Geol 251(1-4):112-119
- Aranovich YL, Newton RC (1996) H₂O activity in concentrated NaCl solutions at high pressures and temperatures measured by the brucite-periclase equilibrium. Contrib Mineral Petr 125:200–212
- Ayers JC, Watson EB (1991) Solubility of Apatite, Monazite, Zircon, and Rutile in Supercritical Aqueous Fluids with Implications for Subduction Zone Geochemistry. Philos T R Soc A 335(1638): 365–375
- Ayers JC, Watson EB (1993) Apatite/fluid partitioning of rare-earth elements and strontium: Experimental results at 1.0 GPa and 1000 °C and application to models of fluid-rock interaction. Chem Geol 110: 299–314
- Belousova E, Griffin W, O'Reilly SY, Fisher N (2002) Apatite as an indicator mineral for mineral exploration: Trace-element compositions and their relationship to host rock type. J Geochem Explor 76(1):45–69
- Betkowski WB, Harlov DE, Rakovan JF (2016) Hydrothermal mineral replacement reactions for an apatite-monazite assemblage in alkalirich fluids at 300–600 °C and 100 MPa. Am Mineral 101(12):2620–2637
- Bingen B, van Breemen O (1998) U-Pb monazite ages in amphibolite- to granulite-facies orthogneiss reflect hydrous mineral breakdown reactions: Sveconorwegian Province of SW Norway. Contrib Mineral Petr 132:336–353
- Boehnke P, Watson EB, Trail D, Harrison TM, Schmitt AK (2013) Zircon saturation re-revisited. Chem Geol 351:324–334
- Brooker RA (1998) Reduction in piston-cylinder experiments: the detection of carbon infiltration into platinum capsules. Am Mineral 83: 985–994
- Chew DM, Petrus JA, Kamber BS (2014) U–Pb LA–ICPMS dating using accessory mineral standards with variable common Pb. Chem Geol 363:185–199
- Dolejš D, Manning CE (2010) Thermodynamic model for mineral solubility in aqueous fluids: Theory, calibration and application to model fluid-flow systems. Geofluids 10:10–20
- Förster H-J, Harlov DE (1999) Monazite-(Ce)- huttonite solid solutions in granulite-facies metabasites from the Ivrea-Verbano Zone, Italy. Mineral Mag 63:587–594
- Frietsch R, Perdahl J-A (1995) Rare earth elements in apatite and magnetite in Kiruna-type iron ores and some other iron ore types. Ore Geol Rev 9:489–510
- Gleadow AJW, Duddy IR, Green PF, Lovering JF (1986) Confined fission track lengths in apatite: A diagnostic tool for thermal history analysis. Contrib Mineral Petr 94:405–415
- Goldoff B, Webster JD, Harlov DE (2012) Characterization of fluorchlorapatites by electron probe microanalysis with a focus on time-dependent intensity variation of halogens. Am Mineral 97(7): 1103–1115
- Harlov DE, Wirth R, Förster H-J (2005) An experimental study of dissolution–reprecipitation in fluorapatite: Fluid infiltration and the formation of monazite. Contrib Mineral Petr 150(3):268–286
- Harlov DE, Wirth R, Hetherington CJ (2011) Fluid-mediated partial alteration in monazite: The role of coupled dissolution–reprecipitation in element redistribution and mass transfer. Contrib Mineral Petr 162(2):329–348
- Hetherington CJ, Harlov DE (2008) Metasomatic thorite and uraninite inclusions in xenotime and monazite from granitic pegmatites, Hidra anorthosite massif, southwestern Norway: Mechanics and fluid chemistry. Am Mineral 93(5–6):806–820



- Hetherington CJ, Harlov DE, Budzyń B (2010) Experimental metasomatism of monazite and xenotime: Mineral stability, REE mobility and fluid composition. Mineral Petrol 99(3–4):165–184
- Hughes JM, Rakovan J (2002) The Crystal Structure of Apatite, Ca5(PO4)3(F,OH,Cl). In: Kohn MJ, Rakovan J, Hughes JM (eds) Phosphates: Geochemical, geobiological, and materials importance. Rev Mineral Geochem, vol 48. Miner Soc Am, Washington DC, pp 1–12
- Leshin LA (2000) Insights into martian water reservoirs from analyses of martian meteorite QUE94201. Geophys Res Lett 27:2017–2020
- Mair P, Tropper P, Harlov DE, Manning CE (2017) The solubility of apatite in H₂O, KCl-H₂O, NaCl-H₂O at 800 °C and 1.0 GPa: Implications for REE mobility in high-grade saline brines. Chem Geol 470:180–192
- Mallmann G, O'Neill HSC (2009) The crystal/melt partitioning of V during mantle melting as a function of oxygen fugacity compared with some other elements (Al, P, Ca, Sc, Ti, Cr, Fe, Ga, Y, Zr and Nb). J Petrol 50(9):1765–1794
- Manning CE, Aranovich LY (2014) Brines at high pressure and temperature: Thermodynamic, Petrogic and geochemical effects. Precambrian Res 253:6–16
- Marks MAW et al (2012) The volatile inventory (F, Cl, Br, S, C) of magmatic apatite: An integrated analytical approach. Chem Geol 291:241–255
- McCubbin FM et al (2010) Nominally hydrous magmatism on the Moon. Proc Natl Acad Sci 107(25):11223–11228
- McCubbin FM et al (2011) Fluorine and chlorine abundances in lunar apatite: Implications for heterogeneous distributions of magmatic volatiles in the lunar interior. Geochim Cosmochim Ac 75(17): 5073–5093
- McCubbin FM, Riner MA, Vander Kaaden KE, Burkemper LK (2012) Is Mercury a volatile-rich planet? Geophys Res Lett 39(9):L09202
- McCubbin FM et al (2014) Volatile abundances of coexisting merrillite and apatite in the martian meteorite Shergotty: Implications for merrillite in hydrous magmas. Am Mineral 99(7):1347–1354
- Miles AJ, Graham CM, Hawkesworth CJ, Gillespie MR, Hinton RW, Bromiley GD (2014) Apatite: A new redox proxy for silicic magmas? Geochim Cosmochim Ac 132:101–119
- Mirwald PW, Kennedy GC (1979) The melting curve of gold, silver, and copper to 60-Kbar pressure: A reinvestigation. J Geophys Res 84: 6750–6756
- Myers J, Eugster HP (1983) The system Fe-Si-O: oxygen buffer calibrations to 1,500K. Contrib Mineral Petr 82:75–90
- Newton RC, Manning CE (2005) Solubility of anhydrite, CaSO₄, in NaCl-H₂O solutions at high pressures and temperatures: Applications to fluid-rock interaction. J Petrol 46(4):701–716
- Newton RC, Manning CE (2010) Role of saline fluids in deep-crustal and upper-mantle metasomatism: Insights from experimental studies. Geofluids 10:58–72
- Paton C, Hellstrom J, Paul B, Woodhead J, Hergt J (2011) Iolite: Freeware for the visualisation and processing of mass spectrometric data. J Anal Atom Spectrom 26:2508–2518
- Piccoli PM, Candela PA (2002) Apatite in igneous systems. In: Kohn MJ, Rakovan J, Hughes JM (eds) Phosphates: Geochemical, geobiological, and materials importance. Rev Mineral Geochem, vol 48. Miner Soc Am, Washington DC, pp 255–292
- Pringle EA, Savage PS, Badro J, Barrat J-A, Moynier F (2013) Redox state during core formation on asteroid 4-Vesta. Earth Planet Sc Lett 373:75–82
- Prowatke S, Klemme S (2006) Trace element partitioning between apatite and silicate melts. Geochim Cosmochim Ac 70:4513–4527
- Ptáček P et al (2016) The field of solid solutions in ternary system of synthetic apatite-type alkaline earth element-yttrium-silicate oxybritholite phases of the composition: AEE_δY_{10-δ}[SiO₄]₆O_{3-0.5δ}, where AEE=Ca, Sr and Ba. Ceram Int 42(5):6154–6167

- Rakovan JF, Hughes JM (2000) Strontium in the apatite structure: strontium fluorapaitite and belovite-(Ce). Can Mineral 38:839–845
- Rakovan JF, McDaniel DK, Reeder RJ (1997) Use of surface-controlled REE sectoral zoning in apatite from Llallagua, Bolivia, to determine a single-crystal Sm-Nd age. Earth Planet Sc Lett 146:329–336
- Richter F, Watson EB, Chaussidon M, Mendybaev R, Ruscitto D (2014) Lithium isotope fractionation by diffusion in minerals. Part 1: Pyroxenes. Geochim Cosmochim Ac 126:352–370
- Rigali MJ, Brady PV, Moore RC (2016) Radionuclide removal by apatite.

 Am Mineral 101(12):2611–2619
- Sarafian AR, Roden MF, Patiño-Douce AE (2013) The volatile content of Vesta: clues from apatite in eucrites. Meteorit Planet Sci 48(11): 2135–2154
- Sato M, Hickling NL, McLane JE (1973) Oxygen fugacity values of Apollo 12 14 and 15 lunar samples and reduced state of lunar magmas. Proceedings of the Fourth Lunar Science Conference, Supplement 4. Geochim Cosmochim Ac 1:1061–1079
- Spear FS, Pyle JM (2002) Apatite, monazite, and xenotime in metamorphic rocks. In: Kohn MJ, Rakovan J, Hughes JM (eds) Phosphates: Geochemical, geobiological, and materials importance. Rev Mineral Geochem, vol 48. Miner Soc Am, Washington DC, pp 293–335
- Stormer JC, Pierson MI, Tacker RC (1993) Variation of F and CI X-ray intensity due to anisotropic diffusion in apatite during electron microprobe analysis. Am Mineral 78:641–648
- Tõnsuaadu K, Gross KA, Plūduma L, Veiderma M (2011) A review on the thermal stability of calcium apatites. J Therm Anal Calorim 110(2):647–659
- Trail D (2018) Redox-controlled dissolution of monazite in fluids and implications for phase stability in the lithosphere. Am Mineral 103:453–461
- Trail D, Watson EB, Tailby ND (2012) Ce and Eu anomalies in zircon as proxies for the oxidation state of magmas. Geochim Cosmochim Ac 97:70–87
- Trail D, Watson EB, Tailby ND (2013) Insights into the Hadean Earth from experimental studies of zircon. J Geol Soc India 81(5):605–636
- Trail D, Cherniak DJ, Watson EB, Harrison TM, Weiss BP, Szumila I (2016) Li zoning in zircon as a potential geospeedometer and peak temperature indicator. Contrib Mineral Petr 171:251–215
- Tropper P, Manning CE, Harlov DE (2011) Solubility of CePO₄ monazite and YPO₄ xenotime in H2O and H2O–NaCl at 800 °C and 1 GPa: Implications for REE and Y transport during high-grade metamorphism. Chem Geol 282(1–2):58–66
- Watson EB (1979) A patite saturation in basic to intermediate magmas. Geophys Res Lett $6{:}937{-}940$
- Watson EB (1980) Apatite and phosphorus in mantle source regions: an experimental study of apatite/melt equilibria at pressures to 25 kbar. Earth Planet Sc Lett 51:322–335
- Watson EB (1987) Diffusion and solubility of C in Pt. Am Mineral 72: 487-490
- Watson EB, Capobianco CJ (1981) Phosphorus and the rare earth elements in felsic magmas: an assessment of the role of apatite. Geochim Cosmochim Ac 45:2349–2358
- Watson EB, Green TH (1981) Apatite/liquid partition coefficients for the rare earth elements and strontium. Earth Planet Sc Lett 56:405–421
- Wohlgemuth-Ueberwasser CC, Tegner C, Pease V (2017) LA-Q-ICP-MS apatite U/Pb geochronology using common Pb in plagioclase: examples from layered mafic intrusions. Am Mineral 102(3):571–579
- Young EJ, Myers AT, Munson EL, Conklin NM (1969) Mineralogy and geochemistry of fluorapatite from Cerro De Mercado, Durango, Mexico. US Geol Surv Prof Pap 650-D:D84–D93
- Zhang C, Koepke J, Albrecht M, Horn I, Holtz F (2017) Apatite in the dike-gabbro transition zone of mid-ocean ridge: evidence for brine assimilation by axial melt lens. Am Mineral 102(3):558–570
- Zolotov MY (2011) On the chemistry of mantle and magmatic volatiles on Mercury. Icarus 212(1):24–41

